Maastricht University

Project Period

Comprehensive Analysis of Bell's Inequality: Classical vs Quantum Computing Study

---

Maastricht Science Programme

2024-2025

Authors:	*ID:*
V. Stefanija	i6295302
T.H. Rohava	i6296714
M.I. Jagielska	i6359915
E. Berna	i6311810
S. Badin	i6291147
M. Miralda Porrero	i6319047
N. Thiessen	i6329841
G.R. Ratajski	i6308360
N. Labuschagne	i6308109

Project Supervisor:

Dr. Keri Vos

23rd January 2025

Contents

1 Abstract

Bell's theorem and the CHSH inequality challenge the classical notion of local hidden variables, providing a critical test for quantum entanglement, a cornerstone ofquantum mechanics and quantum information science. Theoretically and computationally, this project examines the quantum violation of Bell's inequality to highlight the non-local nature of quantum phenomena. Theoretically, the classical bound $|S| \leq 2$ is derived under local-hidden variables. The quantum mechanical bound $|S| \leq 2\sqrt{2}$ is obtained by maximizing the CHSH expression using orthogonal or anti-commuting measurement operators and optimizing vector alignment. The computational analysis, conducted using Qiskit, includes two key experiments. In the first experiment, S is tested for a maximally entangled state by varying the angle θ, demonstrating clear CHSH inequality violations up to the quantum mechanical upper bound and confirming quantum entanglement. In the second experiment, the variation of S with fixed measurement settings for each entanglement angle θ showed periodic violations of the $|S| \leq 2$ threshold, demonstrating the influence of entanglement on the correlation parameter.

2 Introduction

In the early 20th century, the emergence of quantum mechanics challenged classical ideas of reality and determinism. Despite its predictive success, questions about the nature of reality and the completeness of the theory sparked a debate.

In 1935, Eistein, Podolsky and Rosen (EPR) challenged quantum mechanics with a thought experiment grounded in locality and realism. Realism states that physical quantities have definite values, while locality assumes that measurements on one particle do not instantly affect another spatially separated particle. EPR argued that quantum mechanics is incomplete, as it cannot account for predictable correlations between two entangled particles while respecting locality [1].

Building on this critique, in 1952, David Bohm proposed a deterministic hidden variable interpretation of quantum mechanics. Bohm introduced hidden variables, defined as exact positions and momenta of particles determined by the wave function and quantum potential, to provide a deterministic foundation for quantum phenomena, aligning with EPR's call for a more complete theory [2].

In 1964, John Bell further addressed the EPR paradox by translating it into a testable framework through the assumption of locality and the introduction of hidden variables, to model correlations between entangled particles. He derived what is now known as Bell's inequality, which all local hidden variable theories must satisfy [3]. However, Quantum Mechanics predicts correlations for entangled particles that violate Bell's inequality under specific experimental settings, proving that no local hidden variable theory can replicate quantum predictions[3], [4]. Bell concluded that any theory agreeing with quantum mechanics must involve nonlocality [3].

In 1969 Clauser, Horne, Shimony, and Holt (CHSH) extended Bell's work with a practical inequality for realistic experiments. The CHSH inequality defines a classical upper bound $|S| \leq 2$ for correlations under local hidden variable theories [5]. Quantum Mechanics predicts violations of this bound, reaching $|S| \leq 2\sqrt{2}$ in specific configurations, confirming the fundamentally nonlocal nature of quantum mechanics [4], [5].

This project adopts theoretical and computational approaches to provide a comprehensive perspective.

The theoretical component establishes a foundation by introducing quantum systems, defining the correlator E for classical and quantum bounds, and deriving Tsirelson's bound for S using optimization techniques and Hermitian operators.

The computational component involves running two computer programs on quantum hardware and simulators using Qiskit to implement quantum circuits and prepare Bell states. The first code examines measurement settings that maximize *S-values* for maximally entangled states. The second investigates *S-values* for partially entangled states and their sensitivity to measurement settings.

3 Theory

3.1 Quantum States

In quantum mechanics, systems of particle(s) can be found in two different quantum states – pure states and mixed states. In order to clearly describe and discuss quantum entanglement, a solid understanding of these quantum states must be grasped beforehand.

A pure state refers to a system which is in a definite quantum state. If a quantum system is in a pure state, it can be presented as a single *ket* vector $|\psi\rangle$. A pure state which can be written as a combination of product states, such as $|\psi\rangle = |0\rangle \otimes |1\rangle$, is also said to be a separable state since the sub-states it consists of can be expressed individually.

Particles in pure states can also exist in a superposition, as an example:

$$|\psi\rangle = (|0\rangle + |1\rangle)/\sqrt{2}$$

Mixed states are a collection of pure states and do not represent a single definite quantum state. Instead, they are statistical ensembles of two or more states with separate probabilities – although these probabilities can still be the same with one another. For instance, a state which has a probability of $|x|$ to be in $|\psi\rangle$ and a probability of $|y|$ to be in $|\phi\rangle$ is a mixed state. [6]

Although a mixed state might seem to be described the same way as a superposition of states, it is not. A superposition is a state which simultaneously is in multiple other states, whereas a mixed state is a statistical mixture of states.

In entangled quantum systems, by observing the state of one particle (or qubit), the state of the other one can also be immediately known. Entanglement is a property independent of purity and mixedness. Thus, an entangled quantum state can be both. As for experiment 1, the Bell states were used, which are:

$$|\phi^{\pm}\rangle = (|00\rangle \pm |11\rangle)/\sqrt{2}$$
$$|\psi^{\pm}\rangle = (|01\rangle \pm |10\rangle)/\sqrt{2}$$

Referring to the previous explanations, it can be seen that these Bell states are pure and non-separable. Apart from these properties, they are also classified as maximally entangled

states [6]. This means that the entanglement of the particles have not been altered in any way. Therefore, the probabilities of finding a particle in either state are identical, meaning that if you measure an observable of the system in a certain basis, the outcomes for either particle are equally likely.

However, this might not always be the case. If either one of the particles have had an interaction after their separation, then this will affect the outcome of observing a particle in a specific state, causing the probabilities to be different [7]. As an example, partially entangled state can be expressed as:

$$|\phi^{\pm}\rangle = \alpha\,|00\rangle \pm \beta\,|11\rangle$$

where $\alpha \neq \beta$ and $|\alpha|^2 + |\beta|^2 = 1$. [6]

3.2 Classical Bound

The original derivation in J.S. Bell's *Speakable and Unspeakable in Quantum Mechanics* [8] starts with the following setting - two spin - 1/2 particles originating from the same place move into two detector arms A and B. Detector A measures spin of the first particle in the direction of an arbitrary unit vector $\vec{a}$ and detector B measures the spin of the second particle in the direction of an arbitrary unit vector $\vec{b}$.

The theory of local hidden variables then states, that the hypothetical complete description of the initial state of each particle is expressed in terms of a hidden variable λ with a probability distribution $\rho(\lambda)$ for the specific state [8]. The probability distribution is defined as seen in Equation (1), where Λ is the space in which the hidden variables λ are defined [9].

$$\begin{aligned} \int_{\Lambda} \rho(\lambda)\mathrm{d}\lambda &= 1 \\ 0 \leq \rho(\lambda) &\leq 1 \end{aligned} \tag{1}$$

That implies that the result of the measurement A can depend on both $\vec{a}$ and λ. Analogously, result of measurement B can depend on $\vec{b}$ and λ. Since the observable being measured is spin, the result of both of those measurements can only be ± 1. Furthermore, the notion of locality dictates that A does not depend on $\vec{b}$ nor B on $\vec{a}$ [8]. Due to locality, the result of the

measurement of both systems is the product of the results of the separate systems [9]. That way, one defines the expectation value:

$$E\left(\vec{a},\vec{b}\right) = \int_{\Lambda} \rho(\lambda) A\left(\vec{a},\lambda\right) B\left(\vec{b},\lambda\right) \mathrm{d}\lambda \tag{2}$$

To derive an experimentally measurable quantity, one needs to examine the difference between two expectation values, where $\vec{a}'$ and $\vec{b}'$ are alternative settings for the detectors:

$$E\left(\vec{a},\vec{b}\right) - E\left(\vec{a},\vec{b}'\right) = \int_{\Lambda} \rho(\lambda) \left[A\left(\vec{a},\lambda\right) B\left(\vec{b},\lambda\right) - A\left(\vec{a},\lambda\right) B\left(\vec{b}',\lambda\right)\right] \mathrm{d}\lambda \tag{3}$$

Then it's allowed to add and subtract a specific combination of observables A and B. Of course, any arbitrary combination of A and B could be introduced, however this specific one allows for useful factorization in the latter steps and retention of symmetry on the right side of the equation:

$$\begin{aligned} E\left(\vec{a},\vec{b}\right) - E\left(\vec{a},\vec{b}'\right) = \int_{\Lambda} \rho(\lambda) \Big[& A\left(\vec{a},\lambda\right) B\left(\vec{b},\lambda\right) - A\left(\vec{a},\lambda\right) B\left(\vec{b}',\lambda\right) \\ & \pm A\left(\vec{a},\lambda\right) B\left(\vec{b},\lambda\right) A\left(\vec{a}',\lambda\right) B\left(\vec{b}',\lambda\right) \mp A\left(\vec{a},\lambda\right) B\left(\vec{b},\lambda\right) A\left(\vec{a}',\lambda\right) B\left(\vec{b}',\lambda\right) \Big] \mathrm{d}\lambda \end{aligned}$$

That expression can be factorized to simplify:

$$\begin{aligned} E\left(\vec{a},\vec{b}\right) - E\left(\vec{a},\vec{b}'\right) = & \int_{\Lambda} \rho(\lambda) A\left(\vec{a},\lambda\right) B\left(\vec{b},\lambda\right) \left[1 \pm A\left(\vec{a}',\lambda\right) B\left(\vec{b}',\lambda\right)\right] \mathrm{d}\lambda \\ & - \int_{\Lambda} \rho(\lambda) A\left(\vec{a},\lambda\right) B\left(\vec{b}',\lambda\right) \left[1 \pm A\left(\vec{a}',\lambda\right) B\left(\vec{b},\lambda\right)\right] \mathrm{d}\lambda \end{aligned}$$

Then by applying absolute values on both sides of the equation one gets:

$$\left|E\left(\vec{a},\vec{b}\right)-E\left(\vec{a},\vec{b}'\right)\right|=\left|\int_{\Lambda}\rho(\lambda)A\left(\vec{a},\lambda\right)B\left(\vec{b},\lambda\right)\left[1\pm A\left(\vec{a}',\lambda\right)B\left(\vec{b}',\lambda\right)\right]\mathrm{d}\lambda - \int_{\Lambda}\rho(\lambda)A\left(\vec{a},\lambda\right)B\left(\vec{b}',\lambda\right)\left[1\pm A\left(\vec{a}',\lambda\right)B\left(\vec{b},\lambda\right)\right]\mathrm{d}\lambda\right|$$

By utilizing the triangle inequality on the right side of the equation, the expression changes to:

$$\left|E\left(\vec{a},\vec{b}\right)-E\left(\vec{a},\vec{b}'\right)\right|\leq\left|\int_{\Lambda}\rho(\lambda)A\left(\vec{a},\lambda\right)B\left(\vec{b},\lambda\right)\left[1\pm A\left(\vec{a}',\lambda\right)B\left(\vec{b}',\lambda\right)\right]\mathrm{d}\lambda\right| + \left|\int_{\Lambda}\rho(\lambda)A\left(\vec{a},\lambda\right)B\left(\vec{b}',\lambda\right)\left[1\pm A\left(\vec{a}',\lambda\right)B\left(\vec{b},\lambda\right)\right]\mathrm{d}\lambda\right| \quad (4)$$

To find the maximum value of the right side of the equation, the integrand of the first integral can be broken down into three factors:

$$\rho(\lambda) \quad (5)$$

$$A\left(\vec{a},\lambda\right)B\left(\vec{b},\lambda\right) \quad (6)$$

$$\left[1\pm A\left(\vec{a}',\lambda\right)B\left(\vec{b}',\lambda\right)\right] \quad (7)$$

The probability distribution in (5) is by definition non-negative for all λs. Similarly, the expression in Equation (7) is non-negative for all λs. The absolute value of the integral is maximized if the product in (6) has the same value (± 1) over the whole integral. Those statements imply that:

$$\left|\int_{\Lambda}\rho(\lambda)A\left(\vec{a},\lambda\right)B\left(\vec{b},\lambda\right)\left[1\pm A\left(\vec{a}',\lambda\right)B\left(\vec{b}',\lambda\right)\right]\mathrm{d}\lambda\right|\leq \left|\int_{\Lambda}\rho(\lambda)\left[1\pm A\left(\vec{a}',\lambda\right)B\left(\vec{b}',\lambda\right)\right]\mathrm{d}\lambda\right| \quad (8)$$

Applying the same logic to the second integral in Equation (4) and dropping the absolute values outside of the integrals (since the integrands are non-negative) yields:

$$\left|E\left(\vec{a},\vec{b}\right)-E\left(\vec{a},\vec{b}'\right)\right| \leq \int_{\Lambda} \rho(\lambda)\left[1 \pm A\left(\vec{a}',\lambda\right) B\left(\vec{b}',\lambda\right)\right] \mathrm{d}\lambda + \int_{\Lambda} \rho(\lambda)\left[1 \pm A\left(\vec{a}',\lambda\right) B\left(\vec{b},\lambda\right)\right] \mathrm{d}\lambda$$

Each integral is left with two terms now - the integral of $\rho(\lambda)$, which due to Equation (1) reduces to 1, and the product of two observables and $\rho(\lambda)$, which is the original definition of the expectation value E from Equation (2):

$$\left|E\left(\vec{a},\vec{b}\right)-E\left(\vec{a},\vec{b}'\right)\right| \leq 2 \pm \left[E\left(\vec{a}',\vec{b}'\right)+E\left(\vec{a}',\vec{b}\right)\right] \tag{9}$$

Which means that the left side of the equation is less or equal to both $2+\left[E\left(\vec{a}',\vec{b}'\right)+E\left(\vec{a}',\vec{b}\right)\right]$ and $2-\left[E\left(\vec{a}',\vec{b}'\right)+E\left(\vec{a}',\vec{b}\right)\right]$. This can be expressed as:

$$\left|E\left(\vec{a},\vec{b}\right)-E\left(\vec{a},\vec{b}'\right)\right| \leq 2-\left|E\left(\vec{a}',\vec{b}'\right)+E\left(\vec{a}',\vec{b}\right)\right|$$

By using the triangle inequality again, the expression simplifies to:

$$\left|E\left(\vec{a},\vec{b}\right)-E\left(\vec{a},\vec{b}'\right)+E\left(\vec{a}',\vec{b}'\right)+E\left(\vec{a}',\vec{b}\right)\right| \leq 2$$

Taking a coordinate transformation $\vec{a} \rightarrow \vec{a}'$ without the loss of generality, one obtains:

$$\left|E\left(\vec{a},\vec{b}\right)+E\left(\vec{a},\vec{b}'\right)+E\left(\vec{a}',\vec{b}\right)-E\left(\vec{a}',\vec{b}'\right)\right| \leq 2 \tag{10}$$

Or more compactly, by defining a function S:

$$S=E\left(\vec{a},\vec{b}\right)+E\left(\vec{a},\vec{b}'\right)+E\left(\vec{a}',\vec{b}\right)-E\left(\vec{a}',\vec{b}'\right), |S| \leq 2 \tag{11}$$

This is the final form that has been derived by Clauser, Horne, Shimony and Holt [5] and is therefore named the CHSH inequality.

3.3 Quantum Mechanical derivation of E

Equation (12) represent the maximally entangled state $|\Psi\rangle$, where $|ud\rangle$ is defined in Equation (13) as the tensor product between the spin-1/2 particle in spin up measured in detector A and spin down particle measured in detector B.

$$|\Psi\rangle = \frac{1}{\sqrt{2}} \left(|ud\rangle - |du\rangle\right) \tag{12}$$

$$|ud\rangle = |u\rangle_A \otimes |d\rangle_B \tag{13}$$

Then, the expectation value $E\left(\vec{a}, \vec{b}\right)$ is defined in Equation (14), which is the expectation value of the tensor product $(\vec{a} \cdot \vec{\sigma})_A \otimes (\vec{b} \cdot \vec{\sigma})_B$, where $\vec{\sigma}$ is defined as a vector of the Pauli matrices.

$$E\left(\vec{a}, \vec{b}\right) = \langle\Psi| \left(\vec{a} \cdot \vec{\sigma}\right)_A \otimes \left(\vec{b} \cdot \vec{\sigma}\right)_B |\Psi\rangle \tag{14}$$

The product $(\vec{a} \cdot \vec{\sigma})_A$ can be understood as spin operators, which measure the spin in the direction of an arbitrary vector $\vec{a}$ and the subscript A signifies that the operator acts on the first particle from the tensor product in Equation (13). For convenience of notation, it is simplified as $(\vec{a} \cdot \vec{\sigma})_A \equiv \sigma_A$. Substituting Equation (12) into Equation (14) yields:

$$E\left(\vec{a}, \vec{b}\right) = \frac{1}{2} \left(\langle u|_A \otimes \langle d|_B - \langle d|_A \otimes \langle u|_B\right) \otimes \left(\sigma_A |u\rangle_A \otimes \sigma_B |d\rangle_B - \sigma_A |d\rangle_A \otimes \sigma_B |u\rangle_B\right)$$

Now multiplying all the terms:

$$\begin{aligned} E\left(\vec{a}, \vec{b}\right) = \frac{1}{2}\Big[& \left(\langle u|_A \otimes \langle d|_B\right) \otimes \left(\sigma_A |u\rangle_A \otimes \sigma_B |d\rangle_B\right) - \left(\langle u|_A \otimes \langle d|_B\right) \otimes \left(\sigma_A |d\rangle_A \otimes \sigma_B |u\rangle_B\right) \\ & - \left(\langle d|_A \otimes \langle u|_B\right) \otimes \left(\sigma_A |u\rangle_A \otimes \sigma_B |d\rangle_B\right) + \left(\langle d|_A \otimes \langle u|_B\right) \otimes \left(\sigma_A |d\rangle_A \otimes \sigma_B |u\rangle_B\right) \Big] \end{aligned}$$

And combining the products of the same Hilbert spaces A and B:

$$E\left(\vec{a},\vec{b}\right) = \frac{1}{2}\Big[\langle u|_A \sigma_A |u\rangle_A \otimes \langle d|_B \sigma_B |d\rangle_B - \langle u|_A \sigma_A |d\rangle_A \otimes \langle d|_B \sigma_B |u\rangle_B - \langle d|_A \sigma_A |u\rangle_A \otimes \langle u|_B \sigma_B |d\rangle_B + \langle d|_A \sigma_A |d\rangle_A \otimes \langle u|_B \sigma_B |u\rangle_B\Big] \quad (15)$$

Equation (16) showcases how specific Pauli matrices act on spinors $|u\rangle$ and $|d\rangle$.

$$\sigma_x |u\rangle = |d\rangle, \sigma_x |d\rangle = |u\rangle, \sigma_y |u\rangle = i|d\rangle, \sigma_y |d\rangle = -i|u\rangle, \sigma_z |u\rangle = |u\rangle, \sigma_z |d\rangle = -|d\rangle \quad (16)$$

Substituting those values into the expression obtained in Equation (15) and coming back to the definition $(\vec{a}\cdot\vec{\sigma})_A \equiv \sigma_A$, a further simplification is obtained, where a_1, a_2, a_3 are the components of vector $\vec{a}$ and b_1, b_2, b_3 are components of vector $\vec{b}$:

$$E\left(\vec{a},\vec{b}\right) = \frac{1}{2}[a_3(-b_3) - (a_1 - ia_2)(b_1 + ib_2) - (a_1 + ia_2)(b_1 - ib_2)] = -a_1b_1 - a_2b_2 - a_3b_3$$

Which in vector notation reduces to the dot product, which in turn can be expressed as a cosine of the angle between the two vectors (without any factors in front since the vectors are normalized):

$$E\left(\vec{a},\vec{b}\right) = -\vec{a}\cdot\vec{b} = -\cos\theta_{ab} \quad (17)$$

Referring back to Equation (11), the expression for function S in quantum mechanics is:

$$S = -\vec{a}\cdot\vec{b} - \vec{a}\cdot\vec{b'} - \vec{a'}\cdot\vec{b} + \vec{a'}\cdot\vec{b'} \quad (18)$$

3.4 Tsirelson's Bound for S

There are many ways of showing that Quantum Mechanics violates the CHSH inequality. One simple method is to derive the Tsirelson's bound, which implies that for entangled quantum systems, $|S|_{QM} \leq 2\sqrt{2}$ instead of the classical $|S|_C \leq 2$ holds true. [9]

Two derivations will be presented. One involves optimization based on the expectation values established in Section 3.3. Following along the steps found in [9, pp.14-16] and [10,

p.19], the other makes use of Hermitian operators and finds the maximal outcome of a single measurement, as a result of the properties of norms.

3.4.1 Tsirelson's Bound Derivation: Optimization

An advantage of the first approach is that it not only yields the upper bound itself, it also presents the corresponding angles between the detector arms.

For the following optimization, the quantum mechanical expression of S shown in Equation (18) will be utilized. The exact appearance of the vectors is arbitrary, as the coordinate system they are living in can be rotated freely. To simplify, one vector will therefore be defined as a reference for the others: $\vec{a} = \begin{bmatrix} 1 \\ 0 \\ 0 \end{bmatrix}$.

One can now find the values for a_i', b_i and b_i' that maximize S. One way of doing so is to define constraints g_j for the variables and include them in a Lagrangian $\mathcal{L}$ with Lagrange multipliers λ_j. These constraints impose conditions on the outcome based on the physical context, by defining them such that $g_j = 0$. The detector vectors have to be unit vectors:

$$\begin{bmatrix} g_1 \\ g_2 \\ g_3 \\ g_4 \end{bmatrix} = \begin{bmatrix} \sum_{i=1}^{3} |a_i|^2 - 1 = 0 \\ \sum_{i=1}^{3} |a_i'|^2 - 1 = 0 \\ \sum_{i=1}^{3} |b_i|^2 - 1 = 0 \\ \sum_{i=1}^{3} |b_i'|^2 - 1 = 0 \end{bmatrix} = \begin{bmatrix} a_1^2 + a_2^2 + a_3^2 - 1 = 0 \\ {a_1'}^2 + {a_2'}^2 + {a_3'}^2 - 1 = 0 \\ b_1^2 + b_2^2 + b_3^2 - 1 = 0 \\ {b_1'}^2 + {b_2'}^2 + {b_3'}^2 - 1 = 0 \end{bmatrix} \tag{19}$$

Setting up the Lagrangian:

$$\mathcal{L}\left(a_1, a_2, ..., b_3', \lambda_1, ..., \lambda_4\right) = S - \sum_{j=1}^{4} \lambda_j g_j \tag{20}$$

$\mathcal{L}$ depends on 16 variables in total. To find the minimum or maximum value thereof using the method of Lagrange multipliers, if it exists, Equation (20) has to be differentiated wrt. each variable, including the Lagrange multipliers λ_j:

$$\frac{\partial \mathcal{L}}{\partial a_i} = 0 \qquad \frac{\partial \mathcal{L}}{\partial a_i'} = 0 \qquad \frac{\partial \mathcal{L}}{\partial b_i} = 0 \qquad \frac{\partial \mathcal{L}}{\partial b_i'} = 0 \qquad \frac{\partial \mathcal{L}}{\partial \lambda_j} = 0$$

An example of such an equation would be $\frac{\partial \mathcal{L}}{\partial b_1} = -a_1 - a_1' - 2b_1\lambda_3 = 0$. Found in the Appendix, a Python code was developed for an efficient computation and solving process of the

combined equations. C. While several combinations of vectors will satisfy these conditions and maximize S, the angles between the corresponding detector arms will stay the same.

Using this method, Tsirelson's bound can be found:

$$S_{max} = 2\sqrt{2}$$

The angles between the vectors maximizing S are summarized below:

$$\vartheta_{ab} = \vartheta_{ab'} = \vartheta_{a'b'} = \frac{\pi}{4} \qquad \vartheta_{a'b} = \frac{3\pi}{4} \qquad \vartheta_{aa'} = \vartheta_{bb'} = \frac{\pi}{2}$$

Instead of using the dot product notation of S, note that the approach could also have been applied onto the expression for S containing the angles between the vectors. Then, from the beginning already, one could implement the orthogonality between a, a' and b, b' as a physical constraint. However, these calculations are only straightforward under the assumption that all vectors lie in the same plane, meaning that a relation between the four angles can be formulated.

3.4.2 Tsirelson's Bound Derivation: Norms of Hermitian Operators

The main issue with the optimization process lies in the fact that the specific expression for the expectation values E varies with the Bell States ($|\phi^{\pm}\rangle$ and $|\psi^{\pm}\rangle$). The previous derivation utilized the state $|\psi^{-}\rangle = \frac{1}{\sqrt{2}}(|ud\rangle - |du\rangle)$. Although it is not complicated to translate the steps to the other states and reach the Tsirelson's bound, a more general, but less intuitive method inspired by [calltech paper] and [9] will be presented below.

Similar to Section 3.3, the spin operators, correlating to the vectors of the spin measurements, will be defined as follows:

$$\mathbf{a} \equiv (\vec{a} \cdot \vec{\sigma})_A \qquad \mathbf{a'} \equiv (\vec{a'} \cdot \vec{\sigma})_A \qquad \mathbf{b} \equiv (\vec{b} \cdot \vec{\sigma})_B \qquad \mathbf{b'} \equiv (\vec{b'} \cdot \vec{\sigma})_B \tag{21}$$

With $\mathbf{a}$, $\mathbf{a'}$, $\mathbf{b}$ and $\mathbf{b'}$ being observables and thus Hermitian operators, as well as having the eigenvalues ± 1 due to the nature of spin measurements:

$$\mathbf{a}^2 = \mathbf{a'}^2 = \mathbf{b}^2 = \mathbf{b'}^2 = \mathbf{I_2} \tag{22}$$

Above, $\mathbf{I_2}$ is the 2x2 identity matrix. The observables of detector A ($\mathbf{a}$, $\mathbf{a'}$) commute with those of detector B ($\mathbf{b}$, $\mathbf{b'}$), since they are living in different Hilbert spaces, meaning that

measurement of one does not impact measurement of the other. Observables on the same detector cannot commute, since the measurement in one direction collapses the wavefunction and thus affects the results. In commutator form:

$$[\mathbf{a}, \mathbf{b}] = [\mathbf{a}, \mathbf{b}'] = [\mathbf{a}', \mathbf{b}] = [\mathbf{a}', \mathbf{b}'] = 0 \tag{23}$$

$$[\mathbf{a}, \mathbf{a}'] \neq 0 \qquad [\mathbf{b}, \mathbf{b}'] \neq 0 \tag{24}$$

One can now specify an operator combining the different spin measurements, such that a statement about the CHSH inequality can be made:

$$\mathbf{C} = \mathbf{a} \otimes (\mathbf{b} + \mathbf{b}') + \mathbf{a}' \otimes (\mathbf{b} - \mathbf{b}') \tag{25}$$

Before, the calculation for S essentially took the expectation value of this CHSH-Bell operator $\mathbf{C}$, sometimes also denoted by $\mathbf{O_{CHSH}}$. Now, the product between $\mathbf{C}$ and its Hermitian conjugate is computed. Since $\mathbf{C}^\dagger = \mathbf{C}$, the notation can be simplified:

$$\mathbf{C}^2 = [\mathbf{a} \otimes (\mathbf{b} + \mathbf{b}') + \mathbf{a}' \otimes (\mathbf{b} - \mathbf{b}')]^2$$

Expanding the expression:

$$\mathbf{C}^2 = \begin{matrix} \mathbf{a}^2 \otimes \mathbf{b}^2 & +\mathbf{a}^2 \otimes \mathbf{b}\mathbf{b}' & +\mathbf{a}\mathbf{a}' \otimes \mathbf{b}^2 & -\mathbf{a}\mathbf{a}' \otimes \mathbf{b}\mathbf{b}' \\ +\mathbf{a}^2 \otimes \mathbf{b}'\mathbf{b} & +\mathbf{a}^2 \otimes \mathbf{b}'^2 & +\mathbf{a}\mathbf{a}' \otimes \mathbf{b}'\mathbf{b} & -\mathbf{a}\mathbf{a}' \otimes \mathbf{b}'^2 \\ +\mathbf{a}'\mathbf{a} \otimes \mathbf{b}^2 & +\mathbf{a}'\mathbf{a} \otimes \mathbf{b}\mathbf{b}' & +\mathbf{a}'^2 \otimes \mathbf{b}^2 & -\mathbf{a}'^2 \otimes \mathbf{b}\mathbf{b}' \\ -\mathbf{a}'\mathbf{a} \otimes \mathbf{b}'\mathbf{b} & -\mathbf{a}'\mathbf{a} \otimes \mathbf{b}'^2 & -\mathbf{a}'^2 \otimes \mathbf{b}'\mathbf{b} & +\mathbf{a}'^2 \otimes \mathbf{b}'^2 \end{matrix}$$

Using the properties in (22) and canceling equivalent terms:

$$\mathbf{C}^2 = 4\mathbf{I_4} + \mathbf{a}\mathbf{a}' \otimes \mathbf{b}'\mathbf{b} - \mathbf{a}'\mathbf{a} \otimes \mathbf{b}'\mathbf{b} + \mathbf{a}'\mathbf{a} \otimes \mathbf{b}\mathbf{b}' - \mathbf{a}\mathbf{a}' \otimes \mathbf{b}\mathbf{b}'$$

$$\mathbf{C}^2 = 4\mathbf{I_4} - [\mathbf{a}, \mathbf{a}'] \otimes [\mathbf{b}, \mathbf{b}']$$

For Hermitian operators, the operator norm of an operator $\mathbf{M}$ is its maximal eigenvalue. Coincidentally, the aim of Tsirelson's bound is to find the highest possible value for S, that is the maximum eigenvalue of $\mathbf{C}$.

$$||\mathbf{C}^2||_{op} = ||\ (4\mathbf{I_4} - [\mathbf{a}, \mathbf{a'}] \otimes [\mathbf{b}, \mathbf{b'}])\ ||_{op}$$

To proceed, a few properties of norms have to be introduced:

$$||\mathbf{M} \cdot \mathbf{N}||_{op} \leq ||\mathbf{M}||_{op} \cdot ||\mathbf{N}||_{op} \tag{26}$$

$$||\mathbf{M} + \mathbf{N}||_{op} \leq ||\mathbf{M}||_{op} + ||\mathbf{N}||_{op} \tag{27}$$

Relation (26) shows that there exists a combination of operators $\mathbf{M}$ and $\mathbf{N}$, such that one can apply the norm individually on the factors. However, this is also the highest value the operator norm of a product can reach. In relation (27) on the other hand, the triangle inequality is extended to operators.

Applying Relation (27) then gives:

$$||\mathbf{C}^2||_{op} \leq ||4\mathbf{I_4}||_{op} + ||[\mathbf{a}, \mathbf{a'}] \otimes [\mathbf{b}, \mathbf{b'}]||_{op}$$

The commutators involved in the tensor product are independent of each other, so one can apply (26) to further simplify:

$$||\mathbf{C}^2||_{op} \leq 4 + ||[\mathbf{a}, \mathbf{a'}]||_{op} \otimes ||[\mathbf{b}, \mathbf{b'}]||_{op}$$

In the following, the triangle inequality will be brought into play for $||[\mathbf{a}, \mathbf{a'}]||_{op} = ||(\mathbf{aa'} - \mathbf{a'a})||_{op}$. However, the statement $||(\mathbf{aa'} - \mathbf{a'a})||_{op} \leq ||\mathbf{aa'}||_{op} + ||\mathbf{a'a})||_{op}$ includes a combination of $\mathbf{aa'}$ and $\mathbf{a'a}$ that causes the two sides to be equal, which is not obvious due to the value of the two summands being dependent on each other. More precisely, $\mathbf{a}$ and $\mathbf{a'}$ have to anti-commute, which is indeed the case for the Pauli spin matrices σ_X, σ_Y and σ_Z. In other words, the directions of the vectors on the same detector have to be orthogonal to maximize the expectation value of $\mathbf{C}$.

$$||\mathbf{C}^2||_{op} \leq 4 + \left(||\mathbf{aa'}||_{op} + ||\mathbf{a'a}||_{op}\right) \otimes \left(||\mathbf{bb'}||_{op} + ||\mathbf{b'b}||_{op}\right)$$

Lastly, using relation (27) and simplifying:

$$||\mathbf{C}^2||_{op} \leq 4 + \left(||\mathbf{a}||_{op}||\mathbf{a'}||_{op} + ||\mathbf{a'}||_{op}||\mathbf{a}||_{op}\right) \otimes \left(||\mathbf{b}||_{op}||\mathbf{b'}||_{op} + ||\mathbf{b'}||_{op}||\mathbf{b}||_{op}\right)$$
$$||\mathbf{C}^2||_{op} \leq 4 + 4||\mathbf{a}||_{op}||\mathbf{a'}||_{op}||\mathbf{b}||_{op}||\mathbf{b'}||_{op} = 8$$

For the last step, the maximal eigenvalue, 1, was used for each Hermitian operator. Due to the properties of norms, $||\mathbf{C}^2||_{op} = ||\mathbf{C}||_{op}^2$ holds true. Therefore, once again, the derivation of Tsirelson's bound is complete:

$$||\mathbf{C}||_{op} \leq 2\sqrt{2} \tag{28}$$

Furthermore, the maximal value occurs during orthogonality of a, a' and b, b'.

4 Methodology

In order to further investigate the violation of Bell's inequality, three computer programs utilizing Qiskit were developed. They were initially simulated and subsequently tested remotely on real quantum hardware, specifically IBM quantum processing units (QPUs).

4.1 Experimental Computation of S with Varying θ

The first experiment aimed to identify optimal measurement settings for maximizing S-value for a maximally entangled Bell State. The investigation involved varying relative angle θ in order to see when the Tsirelson bound was reached. Measurement bases, in this case, refer to the directions along which quantum states are measured to detect correlations between entangled qubits. For this purpose, a two-qubit circuit, shown in Figure 1, was created. The circuit consists of a Hadamard gate applied to the first qubit (q_0) to induce superposition. Then a controlled NOT (CNOT) gate was applied, using the first qubit as the control and the second qubit (q_1) as the target, generating a maximally entangled pair of qubits. To complete the circuit, a rotation gate around the y-axis ($R_y(\theta)$) was added, where θ represents the rotation angle. Physically, θ corresponds to the angle between the measurement bases. For comprehensive analysis, θ was varied from 0 to 2 π in 21 equal increments.

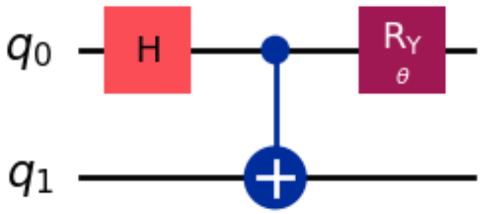

Figure 1: *Two-qubit circuit design with RY gate*

To obtain the expectation values from the CHSH inequality, the terms[1] $\langle A_1B_1\rangle$, $\langle A_1B_2\rangle$, $\langle A_2B_1\rangle$, $\langle A_2B_2\rangle$, corresponding to the observables, were mapped onto the Pauli operators $\langle ZZ\rangle$, $\langle ZX\rangle$, $\langle XZ\rangle$, $\langle XX\rangle$. The Pauli operators represent the projection measurements on different bases, as dictated by the CHSH inequality. Calculating the expectation values for these specific combinations of Pauli operators enables to evaluate the parameter S. Its value determines whether the

[1]There is a change in notation with respect to theory: a is equivalent to A_1, a' is equivalent to A_2, b is equivalent to B_1 and b' is equivalent to B_2

observed correlations surpass the classical limit of 2, as predicted by quantum mechanics. The expected values were then computed with Qiskit's built-in estimator. Using the results obtained and following the CHSH equation, the final values of S were obtained.

Before execution of the code, the circuit was transpiled using Qiskit's built-in commands to optimize its structure, shown in Figure 2. This process generally adjusts the quantum circuit to ensure compatibility with the target simulator's hardware or virtual backend. The program was then run using AerSimulator, and after successful simulation, the experiment was tested on available open-plan QPUs.

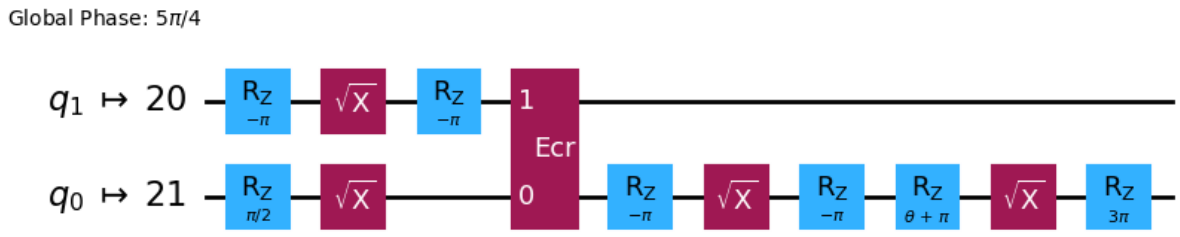

Figure 2: *Transpiled circuit prepared for quantum hardware*

4.2 Experimental Computation of S with Varying Entanglement

The second experiment focused on investigating how a partially entangled quantum system with different measurement settings affects the CHSH inequality. In order to achieve that, two codes were written with the same initial setup but different final steps. In both programs a two-qubit circuit was created followed by the addition of a rotation gate around the y-axis ($R_y(\theta)$) on q_0.

$$|\psi_1\rangle = \cos\left(\frac{\theta}{2}\right)|00\rangle + \sin\left(\frac{\theta}{2}\right)|10\rangle$$

To complete the circuit, a CNOT gate was applied to create entanglement, using q_0 as the control and q_1 as the target. As can be seen in Figure 3.

$$|\psi_2\rangle = \cos\left(\frac{\theta}{2}\right)|00\rangle + \sin\left(\frac{\theta}{2}\right)|11\rangle$$

In this state $\theta = \frac{\pi}{2}$ represents maximum entanglement and $\theta = 0$ represents no entanglement.

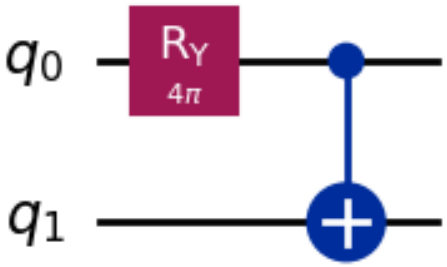

Figure 3: *Two-qubit circuit design with RY gate*

The lack of a Hadamard gate and different order for $R_y(\theta)$ and CNOT, compared to the first experiment, were vital to impose partial entanglement.

Subsequently, a function was developed to investigate the correlation of the quantum state that was not accessible in the standard computational basis (Z-basis) but along different measurement bases. This function could determine these new bases when measurement angles, by which the bases should rotate relative to the Z-basis, were specified. Provided with the set of such measurement angles as input, the function applied Y-axis rotation gates to each qubit, adjusting their measurement bases by the specified amounts. Importantly, each qubit was assigned a distinct local rotation angle, independent of the angle θ that governed partial entanglement. These local rotations did not alter the entangled state itself but reoriented the measurement bases for each qubit. Then, the tensor product of two Pauli Z operators $\langle ZZ \rangle$ was taken as an observable and, using Qiskit's in-built command, allowed to calculate expectation values.

The following figure aims to illustrate the measurement settings examined in this experiment:

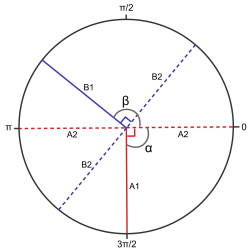

Figure 4: *Possible measurement angles that maximize S. The dashed lines show possible orthogonal combinations for A_2 and B_2, while the angles α and β aim to illustrate the different A_1 and B_1 values explored, from 0 to 2π*

At this stage, the two programs diverge. The first program explored the effect of a fixed set of measurement angles on the correlation between two qubits while varying the level of entanglement with angle θ. The fixed angles were chosen as the canonical settings for maximum CHSH violation in a singlet-like Bell state: $A_1 = 0$, $A_2 = \frac{\pi}{2}$, $B_1 = \frac{\pi}{4}$ and $B_2 = -\frac{\pi}{4}$. Using these angles as inputs to the previously built function, the program computed S values across the entire range of θ.

The second program searched through different sets of measurement angles A_1, A_2, B_1 and B_2 that would maximize the correlation, and thus the S value, at every measured level of entanglement. The code set the constrain of orthogonality between A_1 and A_2 and B_1 and B_2, making the values of A_2 and B_2 dependent on the values of their counterparts: $A_2 = A_1 \pm \frac{\pi}{2}$ and $B_2 = B_1 \pm \frac{\pi}{2}$. Subsequently, multiple loops were applied to iterate through every possible combination of orthogonal A_2 and B_2 values through a list of A_1 values that further iterated through another list of B_1 values. Both lists had values going from 0 to 2π in 32 equal increments, calculating the S value for every possible combination, and only saving the optimal combination for a given level of entanglement. The results of both experiments were visualized using the Matplotlib library.

5 Results and Discussion

5.1 Computation of S with Varying θ

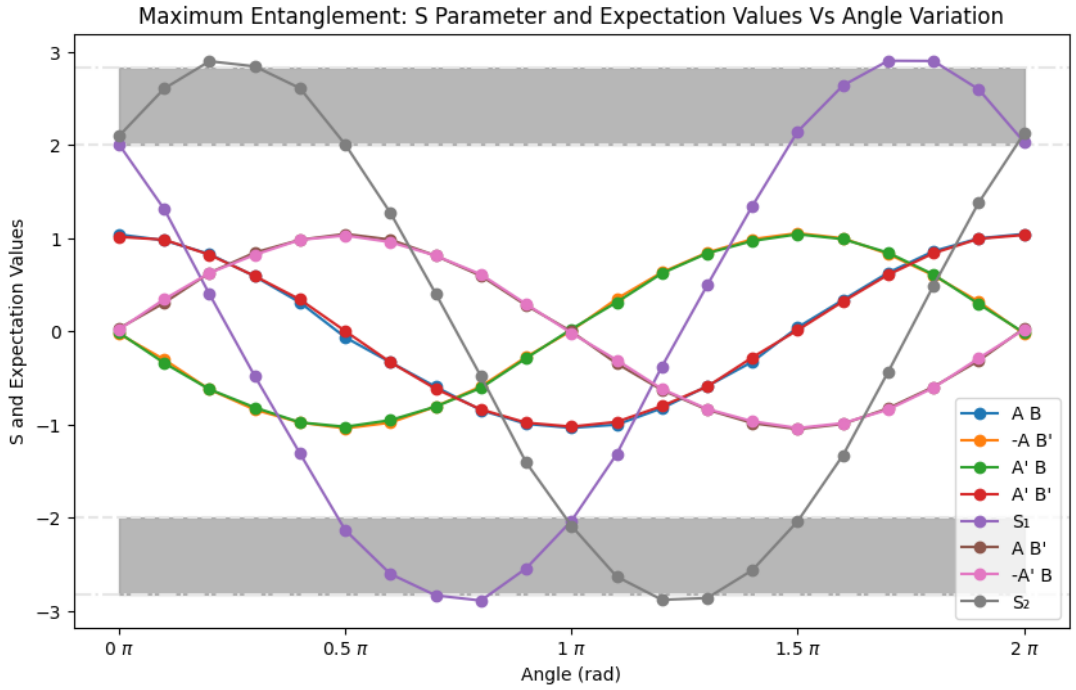

Figure 5: *Impact of Angle Variation on S and Expectation Values Using Quantum Hardware [IBM Brisbane]*

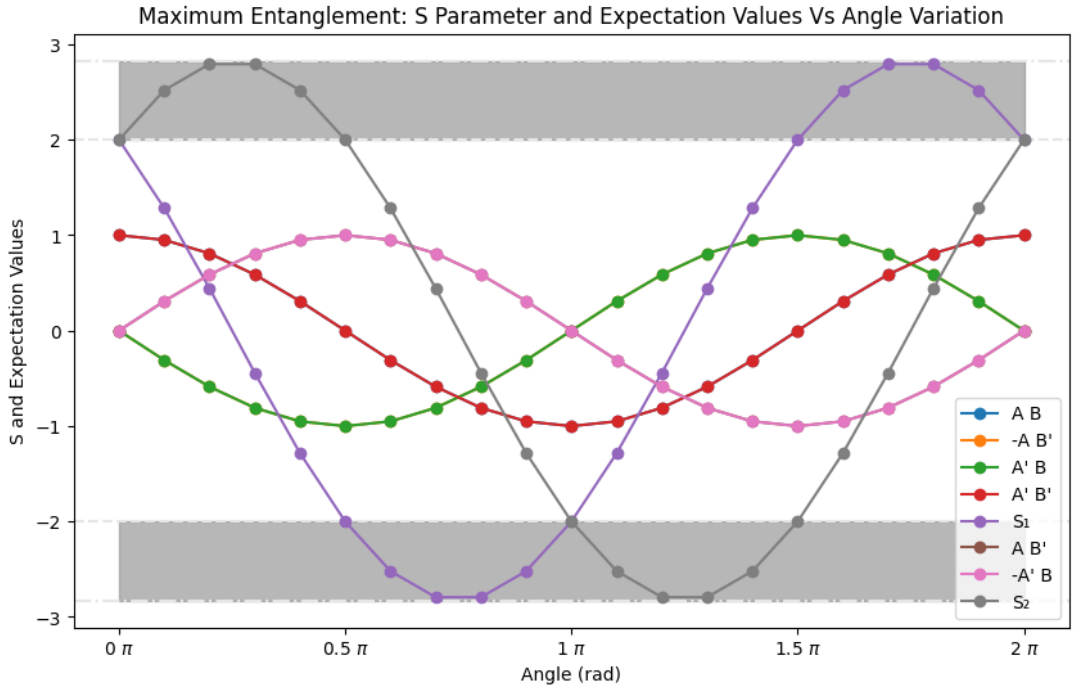

Figure 6: *Impact of Angle Variation on S and Expectation Values Using Simulator*

Figures 5 and 6 illustrate the outcomes of an experiment testing the CHSH inequality on quantum hardware and a quantum simulator, respectively. The graphs show expectation values of various measurement settings and the derived S-parameter as functions of the relative measurement angle θ. A clear violation of the CHSH inequality threshold, $|S| \leq 2$, is observed, with values reaching the quantum mechanical upper bound of $2\sqrt{2} \approx 2.828$. This confirms the presence of quantum entanglement and validates the fundamental prediction that entangled systems exhibit correlations beyond classical limits, in agreement with Bell's theorem [3].

By varying the relative measurement angle θ, Tsirelson's bound was identified when the relative angles between the measurement vectors satisfy the theoretical conditions: $\theta_{ab} = \theta_{ab'} = \theta_{a'b'} = \frac{\pi}{4}$, $\theta_{a'b} = \frac{3\pi}{4}$, and $\theta_{aa'} = \theta_{bb'} = \frac{\pi}{2}$. These angles ensure that the projection operators are optimally aligned on the Bloch sphere, fully exploiting the entanglement properties of the Bell state and underscore orthogonality as a physical constraint [11]. The peaks in the S-parameter ($\theta = \frac{\pi}{4}, \theta = \frac{3\pi}{4}$) on the graphs validate that the experimentally identified optimal measurement settings adhere to the theoretical predictions [12] as discussed in 3.4.1.

The results also reveal the sinusoidal dependence of expectation values on the measurement angle θ, a hallmark of quantum correlations predicted by the inner product of quantum states on the Bloch sphere. For instance, in the CHSH scenario, expectation values follow $\cos(2\theta)$, consistent with the quantum state formalism [12], [13]. These interference effects, absent in classical systems, highlight the non-classical behavior of entangled states.

While results are consistent with theoretical expectations, deviations from the predicted maximum $|S| = 2\sqrt{2}$ are visible in Figure 5, which can be attributed to noise and limitations inherent in current quantum computing hardware. Quantum systems are highly sensitive to external factors, and imperfections in hardware introduce errors at various stages of computation. Specifically, gate errors, caused by inaccuracies in the physical implementation of quantum gates, can lead to deviations in state preparation and operations [14]. Measurement errors, occurring during the process of extracting classical information from quantum states, further contribute to inaccuracies in experimental outcomes [15].

To reduce the impact of noise in this experiment, several techniques could be implemented to enhance the reliability of the results, despite the inherent limitations of current quantum computing hardware. Error mitigation methods, such as zero-noise extrapolation, could be

applied to estimate noiseless outcomes by analyzing results at varying noise levels. Calibration techniques during state preparation and measurement could minimize inaccuracies introduced during qubit initialization and readout [16]. While these approaches can significantly reduce the effects of noise, fundamental limitations, such as short coherence times and high error rates in quantum gates, remain a challenge [14]. Continued advancements in hardware are essential for achieving sound accuracy [17].

Overall, this experiment demonstrates the CHSH inequality's violation on quantum hardware, bridging theoretical quantum mechanics with experimental realization. Figures 5 and 6 are in agreement with prior findings [12], [18], [19], reinforcing the principle of quantum non-locality and confirming that entangled systems exhibit correlations beyond classical limits.

5.2 Computation of S with Varying Entanglement

Figures 7 and 8 illustrate the variation of CHSH S value with fixed and varying measurement settings, respectively, for each θ. The graphs depict the dependence of parameter S on the relative entanglement angle θ and the varied measurement settings that collectively determine the degree of entanglement.

5.2.1 Variation of θ with Fixed Measurement Settings

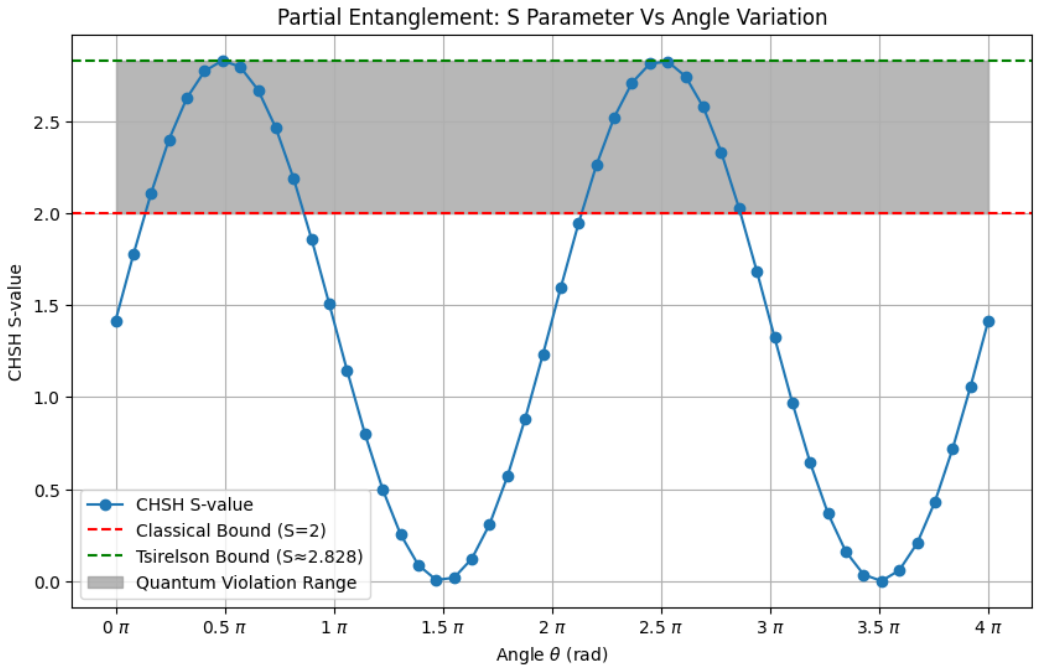

Figure 7: *Impact of Fixed Measurement Settings on Correlation Parameter S with Varying Entanglement*

Figure 7 exhibits a sinusoidal pattern due to the fixed measurement settings periodically exceeding the quantum violation threshold of $|S| \geq 2$. The simulations demonstrate that the chosen measurement angles maximize the correlation when the system reaches maximal entanglement at $\theta = \frac{\pi}{2}$ and minimize it to the greatest extent when there is no entanglement at $\theta = \frac{3\pi}{2}$. Thus, the resulting S values range from 0 to the quantum mechanical upper bound of $2\sqrt{2}$. While this illustrates the influence of the degree of entanglement on the $|S|$ value, it does not capture the maximum achievable $|S|$ for these partially entangled states. Nevertheless, it effectively highlights the distinctions between fully entangled and partially entangled two-qubit systems.

5.2.2 Variation of θ with Measurement Settings Maximizing CHSH Violation

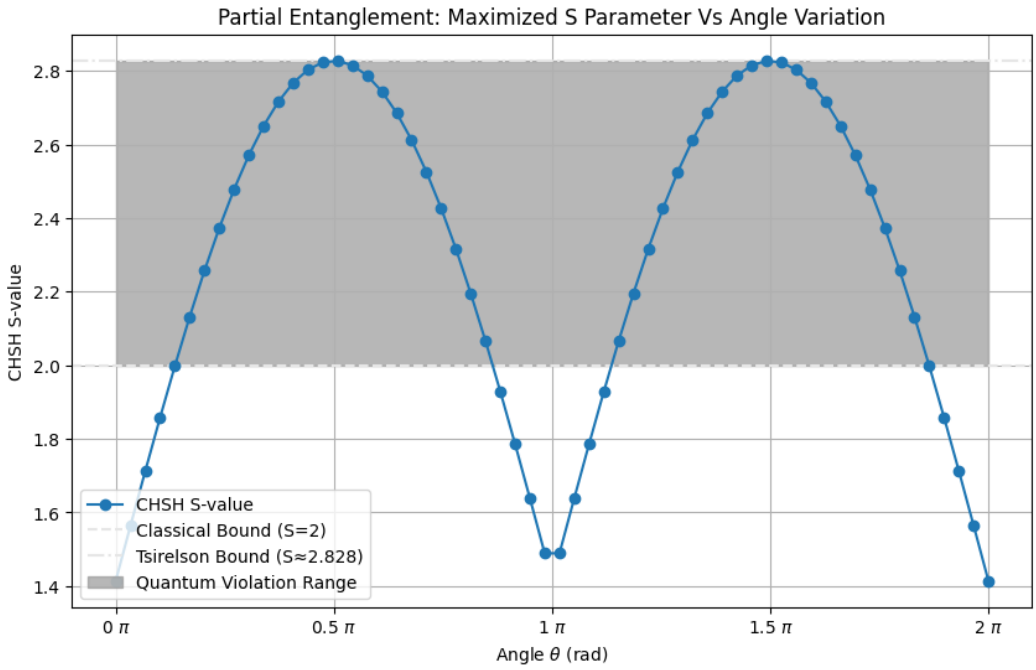

Figure 8: *Impact of Optimal Measurement Settings on Correlation Parameter S with Varying Entanglement*

Figure 8 displays the maximum values of the correlation parameter S for different θ values. The optimized measurement settings modify the correlation parameter S during partial entanglement for optimal results. The outcome of this is represented in moments corresponding to half-entanglement, i.e. at multiples of $\theta = \pi$. Here the trend rebounds into the quantum violation range, eventually reaching the Tsirelson bound again, in contrast to the results from Figure 7.

5.2.3 Optimal Measurement Settings for Each θ

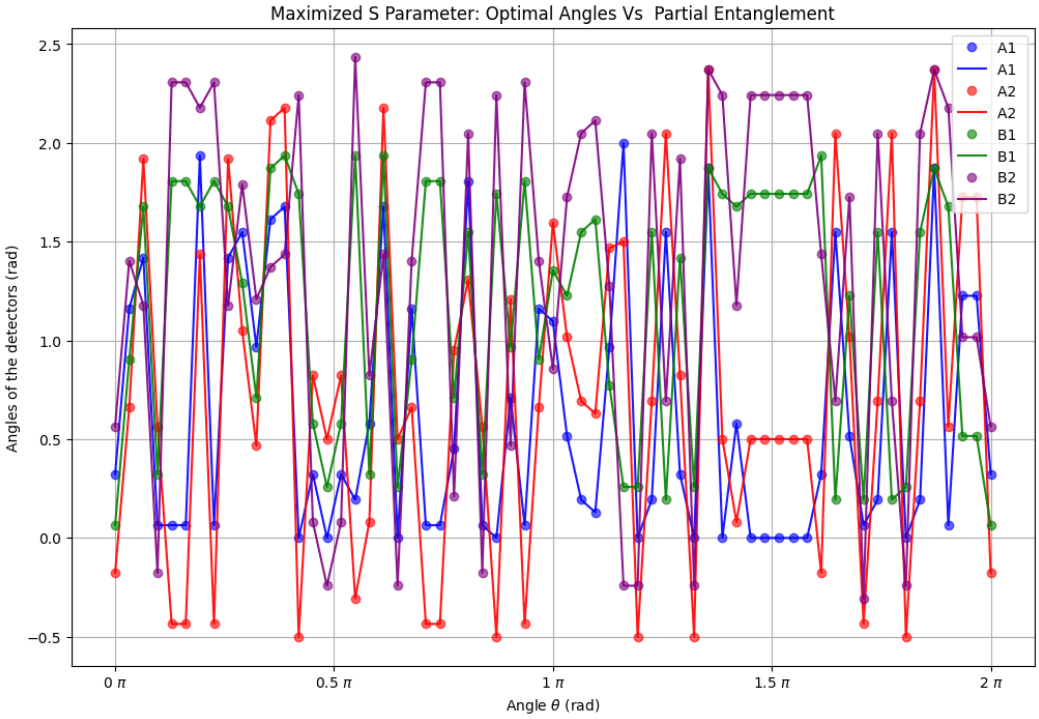

Figure 9: *Impact of Optimal Measurement Settings of the Angles for Maximizing the S Parameter with Varying Entanglement*

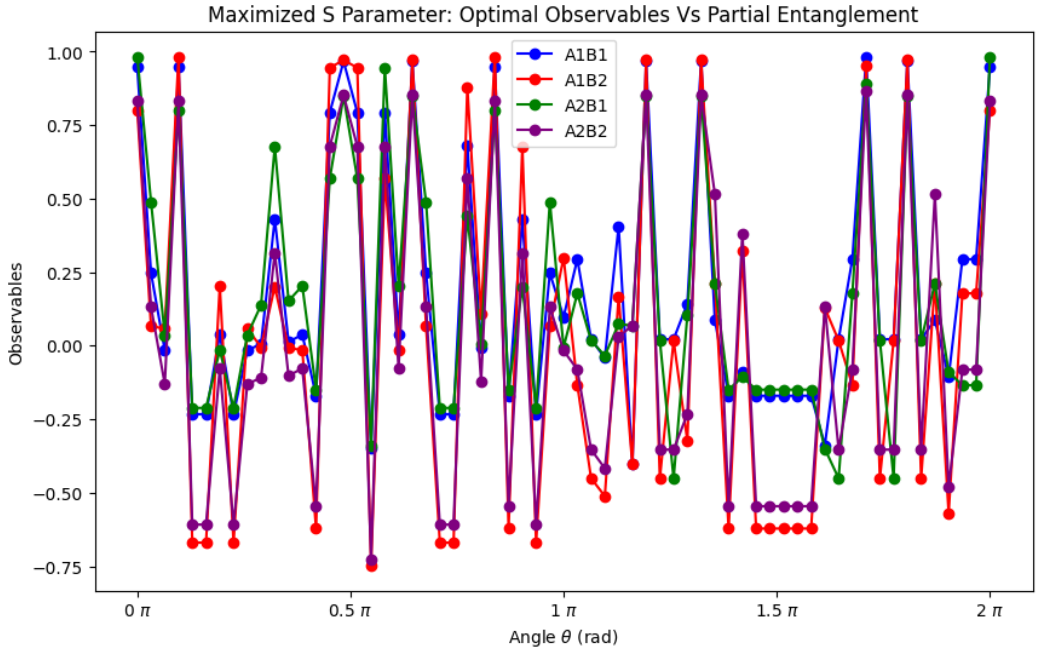

Figure 10: *Impact of Optimal Measurement Settings of the Observables for Maximizing the S Parameter with Varying Entanglement*

Figures 9 and 10 illustrate how after maximizing the settings to obtain the maximum S-value possible, neither the angles (Figure 8) nor the observables (Figure 9) show any visible trends. The chaotic and irregular patterns in the plotted functions highlight the complexity of identifying optimal measurement configurations when dealing with partially entangled states.

There are multiple reasons for this apparent chaos. The code only saved one optimal setting, and there could have been multiple different ones at a given level of entanglement, making specific trends undistinguishable from each other. Another factor to take into account was the limitation in computing power. Due to this, it was unfeasible to check for a bigger list of values for A_2 and B_2, while also calculating many different entanglement levels.

6 Conclusion

This project investigated Bell's inequality, focusing on the CHSH variant and its violations through theoretical derivations and experimental validation. The study highlighted the fundamental differences between classical and quantum correlations, emphasizing quantum mechanical non-locality.

Theoretically, the research employed a systematic approach to derive the classical and quantum bounds for the CHSH inequality. By leveraging optimization techniques and properties of Hermitian Operators, the study confirmed Tsirelson's bound $|S| \leq 2\sqrt{2}$ as upper limit for quantum correlations. These derivations provided a rigorous theoretical framework and a clear benchmark for evaluating experimental results.

The computational component provided a clear evidence for violation of Bell's inequality, using both quantum simulators and real quantum hardware. For maximally entangled states, the observed values of the correlation parameter S approached the quantum mechanical upper limit, confirming the theoretical predictions. The experiments showed how the interplay between entanglement and measurement settings influences the correlation parameter for partially entangled states. While minor deviations from theoretical maxima were observed due to hardware noise, the results consistently aligned with the study's goals.

Overall, this study bridged theoretical predictions with computational outcomes, offering strong evidence for the non-classical behaviour of entangled states. The findings highlight the potential of quantum computing as an infrastructure for exploring the principles of quantum mechanics and provide foundation for future investigations into entanglement and quantum information science. Continued advancements in quantum hardware and error mitigation techniques will further enhance the precision and scope of such studies.

References

[1] A. Einstein, B. Podolsky and N. Rosen, 'Can quantum-mechanical description of physical reality be considered complete?', *Phys. Rev.*, vol. 47, pp. 777–780, 10 May 1935. DOI: 10.1103/PhysRev.47.777. [Online]. Available: https://link.aps.org/doi/10.1103/PhysRev.47.777.

[2] D. Bohm, 'A suggested interpretation of the quantum theory in terms of "hidden" variables. i', *Phys. Rev.*, vol. 85, pp. 166–179, 2 Jan. 1952. DOI: 10.1103/PhysRev.85.166. [Online]. Available: https://link.aps.org/doi/10.1103/PhysRev.85.166.

[3] J. S. Bell, 'On the einstein podolsky rosen paradox', *Physics Physique*, vol. 1, no. 3, pp. 195–200, 1964.

[4] B. S. Cirelson, 'QUANTUM GENERALIZATIONS OF BELL'S INEQUALITY', *Lett. Math. Phys.*, vol. 4, pp. 93–100, 1980. DOI: 10.1007/BF00417500.

[5] J. F. Clauser, M. A. Horne, A. Shimony and R. A. Holt, 'Proposed experiment to test local hidden-variable theories', *Phys. Rev. Lett.*, vol. 23, pp. 880–884, 15 Oct. 1969. DOI: 10.1103/PhysRevLett.23.880. [Online]. Available: https://link.aps.org/doi/10.1103/PhysRevLett.23.880.

[6] T. Jacobson, 'Entanglement and Mixed States', Lecture Notes, University of Maryland, 2018. [Online]. Available: https://physics.umd.edu/grt/taj/623f/QInfo.pdf.

[7] R. Abdelmagid, K. Alshehhi and G. Sadiek, 'Entanglement degradation in two interacting qubits coupled to dephasing environments', en, *Entropy (Basel)*, vol. 25, no. 10, Oct. 2023.

[8] J. S. Bell and A. Aspect, *Speakable and Unspeakable in Quantum Mechanics: Collected Papers on Quantum Philosophy*, 2nd ed. Cambridge University Press, 2004.

[9] A. Kaarna, 'Tsirelson's bound Introduction and Examples', Bachelor's Thesis, Karlstads Universitet, 2022-05-31.

[10] J. Preskill, 'Quantum Information and Computation Chapter 4', Lecture Notes, California Institute of Technology, 2001-11-02. [Online]. Available: http://theory.caltech.edu/~preskill/ph229/notes/chap4_01.pdf.

[11] R. Horodecki *et al.*, 'Quantum entanglement', *Reviews of Modern Physics*, vol. 81, no. 2, p. 865, 2009.

[12] A. Aspect, J. Dalibard and G. Roger, 'Experimental test of bell's inequalities using time-varying analyzers', *Physical Review Letters*, vol. 49, no. 25, p. 1804, 1982.

[13] N. D. Mermin, 'Hidden variables and the two theorems of john bell', *Reviews of Modern Physics*, vol. 65, no. 3, p. 803, 1993.

[14] U. Aseguinolaza, N. Sobrino, G. Sobrino, J. Jornet-Somoza and J. Borge, 'Error estimation in current noisy quantum computers', *Quantum Information Processing*, vol. 23, no. 5, May 2024, ISSN: 1573-1332. DOI: 10.1007/s11128-024-04384-z. [Online]. Available: http://dx.doi.org/10.1007/s11128-024-04384-z.

[15] A. Kandala, K. Temme, A. D. Córcoles, A. Mezzacapo, J. M. Chow and J. M. Gambetta, 'Error mitigation extends the computational reach of a noisy quantum processor', *Nature*, vol. 567, no. 7749, pp. 491–495, 2019.

[16] H. Sohn, J. Jung, J. Park *et al.*, *Application of zero-noise extrapolation-based quantum error mitigation to a silicon spin qubit*, 2024. arXiv: 2410.10339 [quant-ph]. [Online]. Available: https://arxiv.org/abs/2410.10339.

[17] S. Resch and U. R. Karpuzcu, 'Benchmarking quantum computers and the impact of quantum noise', *ACM Computing Surveys (CSUR)*, vol. 54, no. 7, pp. 1–35, 2021.

[18] A. K. Ekert, 'Quantum cryptography based on bell's theorem', *Physical Review Letters*, vol. 67, no. 6, p. 661, 1991.

[19] *Chsh inequality tutorial*, https://learning.quantum.ibm.com/tutorial/chsh-inequality, Accessed: January 21, 2025.

7 Appendix

The following link provides access to the GitHub repository containing all the code used in this project:

Bells Inequality SLP Repository.

7.1 Dependence of Expectation Values with varied θ

Angle (rad)	A_1B_1	$-A_1B_2$	A_2B_1	A_2B_2	A_1B_2	$-A_2B_1$
0.0000	1.0373	-0.0290	-0.0167	1.0123	0.0290	0.0167
0.3142	0.9749	-0.3049	-0.3428	0.9816	0.3049	0.3428
0.6283	0.8266	-0.6260	-0.6249	0.8199	0.6260	0.6249
0.9425	0.5886	-0.8428	-0.8194	0.5914	0.8428	0.8194
1.2566	0.3077	-0.9805	-0.9799	0.3395	0.9805	0.9799
1.5708	-0.0663	-1.0429	-1.0268	0.0006	1.0429	1.0268
1.8850	-0.3350	-0.9822	-0.9554	-0.3344	0.9822	0.9554
2.1991	-0.5975	-0.8094	-0.8099	-0.6198	0.8094	0.8099
2.5133	-0.8484	-0.5936	-0.6093	-0.8406	0.5936	0.6093
2.8274	-0.9955	-0.2770	-0.2904	-0.9827	0.2770	0.2904
3.1416	-1.0379	0.0050	0.0217	-1.0251	-0.0050	-0.0217
3.4558	-1.0039	0.3473	0.3099	-0.9738	-0.3473	-0.3099
3.7699	-0.8272	0.6315	0.6210	-0.8043	-0.6315	-0.6210
4.0841	-0.5914	0.8428	0.8356	-0.5953	-0.8428	-0.8356
4.3982	-0.3283	0.9872	0.9682	-0.2815	-0.9872	-0.9682
4.7124	0.0401	1.0518	1.0401	0.0111	-1.0518	-1.0401
5.0265	0.3344	0.9967	0.9883	0.3177	-0.9967	-0.9883
5.3407	0.6271	0.8283	0.8417	0.6054	-0.8283	-0.8417
5.6549	0.8573	0.5987	0.6081	0.8361	-0.5987	-0.6081
5.9690	0.9955	0.3172	0.2915	0.9916	-0.3172	-0.2915
6.2832	1.0429	-0.0279	-0.0162	1.0323	0.0279	0.0162

Table 1: Measurement Outcomes for the Observables at Different Angles

7.2 Contributions

Column 1	**Column 2**
Tatsiana	Writing Introduction, Abstract, Conclusion
Vita Stefanija	Coding 5.1, 5.2, Writing 5.1
Magda	Coding 5.1, 5.2, Result Collection, Writing 4 and 5.2
Miguel	Contribution 4.2, Writing 5.2.3, Coding and Plotting 5.1 and 5.2, Running 5.1 on Quantum Hardware, Result Collection, Designed Figure 3 and the Methodology Involved
Nils	Writing 3.4, Contribution 3.3
Grzegorz Ratajski	Writing 3.2, 3.3
Emre Berna	Writing 3.1
Samuel Badin	Writing 4.1, Contribution 5.2

Table 2: Contributions of team members